Applied Catalysis B: Environmental 140–141 (2013) 115–124

Contents lists available at SciVerse ScienceDirect

Applied Catalysis B: Environmental

journal homepage: www.elsevier.com/locate/apcatb

A highly efficient heterogeneous catalyst of Ru/MMT: Preparation, characterization, and evaluation of catalytic effect

Shuge Peng, Xinjie Fan, Jun Zhang, Fayuan Wang*

Key Laboratory of Polymer and Nanomaterials, College of Chemical Engineering and Pharmacy, Henan University of Science and Technology, Luoyang 471003, PR China

ARTICLE INFO

Article history:
Received 14 February 2013
Received in revised form 11 March 2013
Accepted 17 March 2013
Available online 26 March 2013

Keywords:
Hydrogen generation
Ruthenium nanoparticles
Montmorillonite
Sodium borohydride

ABSTRACT

This study focuses on the evaluation of the catalyst activity and reutilization in the catalyzed hydrolysis of sodium borohydride ($NaBH_4$). To date, few studies on reutilization are available in literature. In the present study, a facile method was used to obtain a highly efficient catalyst, Ru nanoparticles deposited on external surface of montmorillonite (Ru/MMT). Catalytic activity and reutilization were evaluated by analyzing the H_2 generation rate from an alkaline $NaBH_4$ solution. The catalytic activity of the as-prepared Ru/MMT was determined as a function of the catalyst amount, $NaBH_4$ concentration, and temperature. By using the as-prepared Ru/MMT catalyst with a concentration of 1 wt% $NaBH_4$, an average hydrogen generation rate as high as $28{,}500 \pm 500\ mL\ min^{-1}\ g(Ru)^{-1}$ is achieved at 25 °C. The kinetic study demonstrates that the hydrolysis reaction is first-order in terms of the catalyst concentration and zero-order in terms of the substrate concentration. The apparent activation energy of $NaBH_4$ hydrolysis is 54.7 ± 1 kJ/mol, which is lower than most Ru-based catalysts reported in literatures. However, the catalytic activity of the reused catalyst dramatically decreased, with only 49% of the initial H_2 generation rate remaining after 10 runs. The degradation mechanism of the Ru/MMT catalyst during cycling was investigated and discussed in detail. Before and after 10 reutilizations, the textural properties of the catalysts were characterized based on the nitrogen adsorption–desorption isotherms (obtained using Brunauer–Emmett–Teller analysis), the surface morphology (obtained using field-emission scanning electron microscopy, and transmission electron microscopy), and on the surface composition (obtained using energy-dispersive X-ray spectroscopy, elemental analysis, and X-ray photoelectron spectroscopy). The deterioration of the reused catalyst seemed to be caused by the aggregation and partial fall-off of the Ru nanoparticles deposited on the MMT external surface.

1. Introduction

Energy conservation and environmental protection are recognized as the core elements of sustainable development. Highly efficient, easy-to-use fuel cells with low environmental impact have attracted considerable attention, particularly with the increasing population and greenhouse gas emissions worldwide [1]. The proton-exchange membrane fuel cell (PEMFC) is a promising attractive alternative power source because of its high performance at low temperatures [2]. However, safe and efficient H_2 production and storage is the key to PEMFC commercialization. To date, studies on on-board H_2 production, such as the use of compressed gas, adsorption on carbon materials, as well as the use of metal hydrides and chemical hydrides, have attracted increasing attention and achieved a number of significant results [3]. Of these H_2 storage systems, the hydrolysis of chemical hydrides is receiving particular attention as an ideal source of pure H_2 for PEMFCs [4]. Considerable attention has been focused on the hydrolysis of sodium borohydride ($NaBH_4$) because of its relatively safe and high hydrogen content [5,6]. In addition, $NaBH_4$ is very stable in alkaline solutions, only if the solution is in contact with specific catalysts [7]. A number of substances have been found effective in accelerating $NaBH_4$ hydrolysis, such as noble metal [8–10], non-noble metal [11–14], metal compounds [15–19], and metal alloy [20–22], etc. Precious metal catalysts such as those of Pt (0), Rh (0), and Ru (0) were found to exhibit significantly higher activities than non-noble metal catalyst [23]. Ru has a price advantage among the precious metals. Therefore, Ru-based catalysts remain the preferred choice in building highly efficient catalysts for $NaBH_4$ hydrolysis [24–27].

Catalyst supports can significantly affect the catalytic performance of metal catalysts [28]. Nowadays, the supports used for $NaBH_4$ hydrolysis mainly focused on some conventional supports such as activated carbon (C), aluminum oxide (Al_2O_3), and ion-exchange resins. Some supports with ordered structures have not

* Corresponding author. Tel.: +86 379 64282340; fax: +86 379 64282340.
E-mail address: wfy1975@163.co (F. Wang).

0926-3373/$ – see front matter © 2013 Elsevier B.V. All rights reserved.
http://dx.doi.org/10.1016/j.apcatb.2013.03.029

received sufficient attention in investigations on $NaBH_4$ hydrolysis. For example, one of the available natural materials that can be often used in heterogeneous catalysis is the clay mineral [29]. Montmorillonite (MMT), a naturally occurring, nonhazardous clay mineral composed of layers of negatively charged two-dimensional magnesium aluminum silicates that are charge-balanced by interlayer alkali or alkaline earth metal cations. Compared with other reported supports for $NaBH_4$ hydrolysis, MMT have several obviously advantages over other support matrices: (1) MMT is abundant worldwide and more inexpensive; (2) MMT has even more open framework structure than other porous materials and does not cause significant mass-transfer limitation; (3) MMT has much higher chemical and heat stability than organic supports; and (4) the electrostatic force between MMT and metal nanoclusters is stronger than the physical absorption existed in other porous supports. Due to all the advantages, MMT has been widely used as a support to construct novel nanocomposites, which are of great potential in many practical applications such as catalysis, adsorption, and environmental remediation [30–32]. However, only few researchers reported the application of MMT in the hydrolysis of chemical hydrides [33–35]. Actually, a number of questions remain to be addressed, such as the interaction between guest nanoparticles and the matrix, the effects of surfaces on the supported guest nanoparticles, and the physical and chemical processes underlying the activity loss, among others. Thus, increased attention should be focused on this field.

To develop a high-activity catalyst for the $NaBH_4$ hydrolysis, it is indispensable to improve the dispersibility of Ru nanoclusters on the surface of support. This clay mineral is, thus, expected to be suitable to stabilize Ru nanoclusters as well as favoring the reuse and recycling of nanoparticles from reaction mixtures. From this point of view, the Ru/MMT is promising as an environmental-friendly heterogeneous catalyst. The objectives of this study were to prepare Ru nanoclusters deposited on the external surface of MMT and to investigate the catalytic activity and reutilization of the catalyst evaluated from the alkaline $NaBH_4$ hydrolysis. The catalytic kinetics of $NaBH_4$ hydrolysis, and the reusability of the catalyst, were studied and discussed in more detail. To our knowledge, no reports on the use of Ru/MMT catalyst in the catalytic hydrolysis of an alkaline $NaBH_4$ solution have been published to date, particularly on the degradation mechanism of Ru/MMT during repeated use.

2. Experimental

2.1. Materials

Ruthenium chloride hydrate ($RuCl_3 \cdot nH_2O$, Ru content $\geq$37%) was obtained from Aldrich and used as-received. Montmorillonite with a cation-exchange capacity (CEC) of approximately 60 meq/100 g to 70 meq/100 g was obtained from Zhejiang, China; $NaBH_4$ and NaOH were purchased from Sinopharm Chemical Reagent Co. Ltd. Deionized water was prepared using a water purification system.

2.2. Catalyst preparation

Na-MMT was first purified by sedimentation. The chemical composition of the purified MMT was 64.6 wt% SiO_2, 21.7 wt% Al_2O_3, 6.3 wt% Fe_2O_3, 3.9 wt% MgO, 1.2 wt% CaO, 0.7 wt% K_2O, and 1.6 wt% Na_2O, as determined using X-ray fluorescence (XRF). Fig. 1 illustrates the preparation procedure of the Ru/MMT catalyst. In a typical run, 5.0 g purified Na-MMT was dispersed in 200 mL of an aqueous $RuCl_3$ solution (2 wt% of Ru with respect to the clay weight) via ultrasonication for 5 min and then magnetically stirred at room temperature for 2 h, which was subsequently reduced by the addition of KBH_4 powder (0.5 g). After KBH_4 was added, the solution turned black quickly, indicating the reduction of Ru^{3+}. The Ru/MMT powder was collected by filtration and then thoroughly washed with deionized water to remove the excess salt. The powder was then dried at 110 °C for 10 h and subsequently ground into a fine powder.

2.3. Catalyst characterizations

Powder X-ray diffraction (XRD) analysis was carried out with a Rigaku D/MAX-2200 diffraction using Ni-filtered Cu Kα radiation. TEM images were observed from a JEOL JSM-200CX transmission electron microscope. Morphology and elemental composition analysis of the catalyst were obtained with a field emission scanning electron microscopy (FESEM, Hitachi S 4800) coupled with EDX. X-ray photoelectron spectroscopy (XPS) of the catalyst was collected on a VG Scientific ESCALAB 200 A spectrometer to analyze the electronic state of the surface elements. Ru content in catalyst was estimated using a PROFILE SPEC inductive coupled plasma emission spectrometer (ICP). The determination of surface areas (S_{BET}), by N_2 adsorption–desorption were measured at 77 K using the Micromeritics ASAP 2020 adsorption analyzer. Prior to measurements, the samples were degassed at 423 K in vacuum for 5 h.

2.4. Catalyst evaluation

The catalytic activity of the Ru/MMT catalyst was determined by measuring the amount of H_2 generation from the hydrolysis of an alkaline $NaBH_4$ solution using a modified water displacement method. A three-necked flask containing a Teflon-coated stir bar, Ru/MMT catalysts, and $NaBH_4$ powder was placed on a magnetic stirrer. A graduated glass tube filled with water was connected to the three-necked flask to measure the volume of H_2 generated by the hydrolysis reaction. A 10 mL NaOH solution was then rapidly injected into the three-necked flask using a glass syringe under vigorous stirring to initiate the catalytic hydrolysis of $NaBH_4$. The starting point of the catalytic reaction was defined as the time when the NaOH solution was injected into the flask. The volume of H_2 evolved was measured by recording the displacement of the water level under constant pressure. During the measurement, the solution temperature was measured and carefully controlled within ±0.5 °C.

A series of experiments were performed to establish the rate law of the $NaBH_4$ hydrolysis as catalyzed by Ru/MMT. The hydrolysis reaction was performed starting with different amounts of Ru/MMT (8, 16, 24, and 32 mg) while keeping the $NaBH_4$ amount (0.1 g) and the NaOH concentration (3 wt%) constant. The hydrolysis reaction was then performed by keeping the Ru/MMT amount (8 mg) and NaOH concentration (3 wt%) constant but varying the $NaBH_4$ concentrations (1, 3, 5, and 10 wt%). To determine the activation energy (E_a), the Ru/MMT-catalyzed $NaBH_4$ hydrolysis was performed using constant Ru/MMT (32 mg) and $NaBH_4$ (0.1 g) amounts as well as a constant NaOH concentration (3 wt%) under different temperatures (ranging from 10 °C to 30 °C).

3. Results and discussion

3.1. Preparation, morphologies and structures of the Ru/MMT catalyst

This investigation aims to develop a simple and efficient method for preparing Ru/MMT nanocomposites as catalysts for the H_2 generation from an alkaline $NaBH_4$ solution. As illustrated in Fig. 1, Ru^{3+} ions were not able to be intercalated directly into the galleries of Na-MMT. Because of the strong combination between Ru^{3+} and

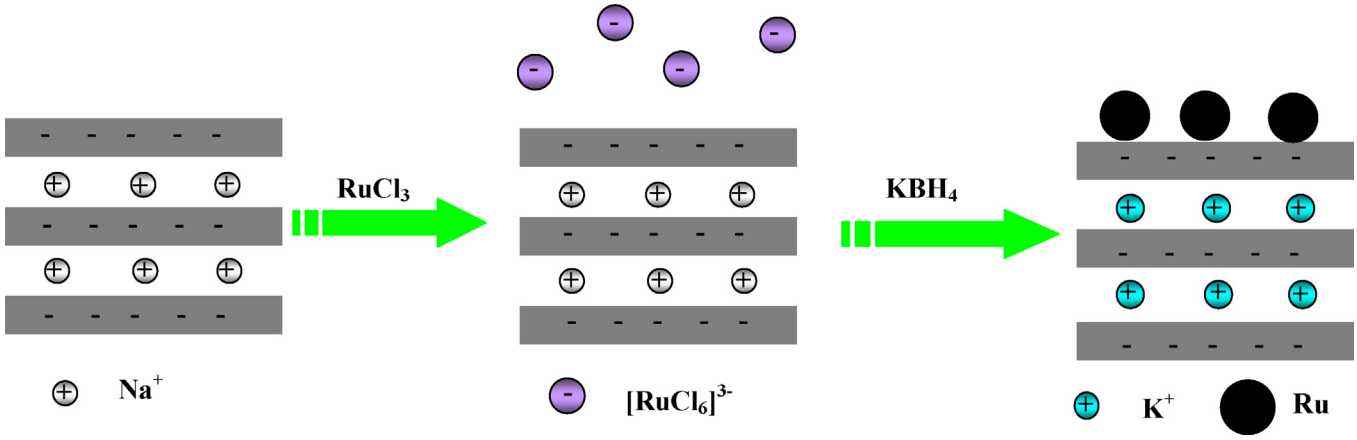

Fig. 1. Illustration of the preparation procedure of the Ru nanoparticles deposited in the MMT matrix (Ru/MMT).

Cl^- ions to form anionic complexes, e.g. $[RuCl_6]^{3-}$ in $RuCl_3$ solution [36], and they have little or no attraction for MMT having negatively charged silicate sheets. Thus, Ru nanoculsters could be deposited on the external surface of MMT during the reduction process in the presence of Na-MMT as an effective stabilized reagent and support as well. Recently, a similar study was reported by Fan et al. [37], who also obtained Fe nanoparticles deposited on the external surface of MMT with borohydride reduction method.

The XRD patterns of the Na-MMT and as-prepared Ru/MMT samples in the small-angle range are presented in Fig. 2. The basal spacing of Na-MMT was 1.30 nm, whereas that of Ru/MMT was enlarged to d_{001} = 1.44 nm according to the Bragg equation ($2d\sin\theta = n\lambda$, λ = 0.15406 nm). The 0.14 nm expansion is attributed to the incorporation of K^+ into the MMT galleries. The XRD result clearly proved that Ru nanoparticles could not go into the MMT interlayers, and mainly occupy the external surface of clay. Moreover, no characteristic diffraction peak appeared for the Ru nanoparticles in the wide-angle XRD pattern, implying that the deposited Ru nanoparticles on the external surface were either very small or amorphous.

Substantial evidences for the existence of Ru nanoclusters in MMT are still being investigated. The TEM image (Fig. 3a) of the as-prepared Ru/MMT catalyst, obtained by borohydride reduction

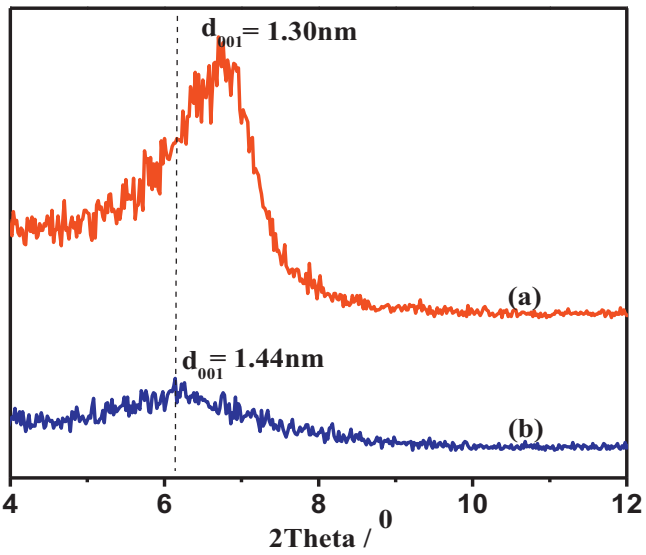

Fig. 2. XRD patterns of the Na-MMT (a), and as-prepared Ru/MMT catalyst (b).

of ruthenium salt in the presence of Na-MMT as a stabilized reagent and support as well, shows dark particles that are randomly distributed in the MMT matrix. These dark particles were assumed to be Ru nanoparticles on the external MMT surface because the EDX results (Fig. 3c) clearly show the presence of elemental Ru in the catalyst sample. Additionally, the corresponding selected area electron diffraction (SAED) pattern of the sample (Fig. 3b) shows broad rings, indicating that nanocrystalline phase are present in agreement with the XRD result. The two diffraction rings correspond to *d*-spacing of 1.93 and 1.21 Å, respectively. The values fit the reflections of the (1 0 1) and (1 0 3) lattice planes of hexagonal close packed metal Ru [38]. The size distribution of the deposited Ru nanoparticles is shown in Fig. 3(d). The results indicate that the particle size of the deposited Ru nanoparticles ranged from 1.2 nm to 8.8 nm, with a mean value of approximately 3.9 nm, implying a high monodispersity of the Ru nanoclusters. Notably, small agglomerations also exist, which might result from the heterogeneous surface activities of the clay used. The TEM results confirm the deposition of Ru nanoparticles on the external surface of MMT, which is consistent with the XRD results.

To confirm the formation of metallic Ru(0) nanostructures further, XPS measurements were used to determine the oxidation state of the Ru nanopraticles deposited on MMT (Fig. 4). As shown in Fig. 4(a), the binding energies of Ru/MMT at 483.7, and 460.8 eV are attributed to the binding energies of Ru $3p_{1/2}$ and Ru $3p_{3/2}$, respectively, which are consistent with those of Ru metal [39]. Moreover, the presence of a Ru—O component was observed in the deconvoluted spectrum of Ru 3d except Ru^0 in the as-prepared catalyst (Fig. 4b). The presence of Ru—O component probably results from the partially oxidation of the Ru nanoparticles upon exposure to air at room temperature, which in turn enhances the interaction between Ru nanoparticles and support.

EDX analysis (Fig. 3c) indicated that Ru nanoparticles were deposited on the surface of MMT. The accurate experimental amount of Ru in the MMT matrix was measured using ICP. As listed in Table 2, the Ru content in the as-prepared Ru/MMT catalyst was found to be 1.91 wt%, which was nearly close to 2 wt%, the experimental amount of Ru in MMT. The method minimized the loss of Ru metal nanoparticles during synthesis.

3.2. Evaluation of the catalytic activity

$NaBH_4$ solutions are generally stable when maintained at high pH [40]. However, in this study, the hydrolysis rate markedly increased at 25 °C in the presence of Ru/MMT catalyst even at high pH solutions. This result shows that the H_2 generation rate (HGR)

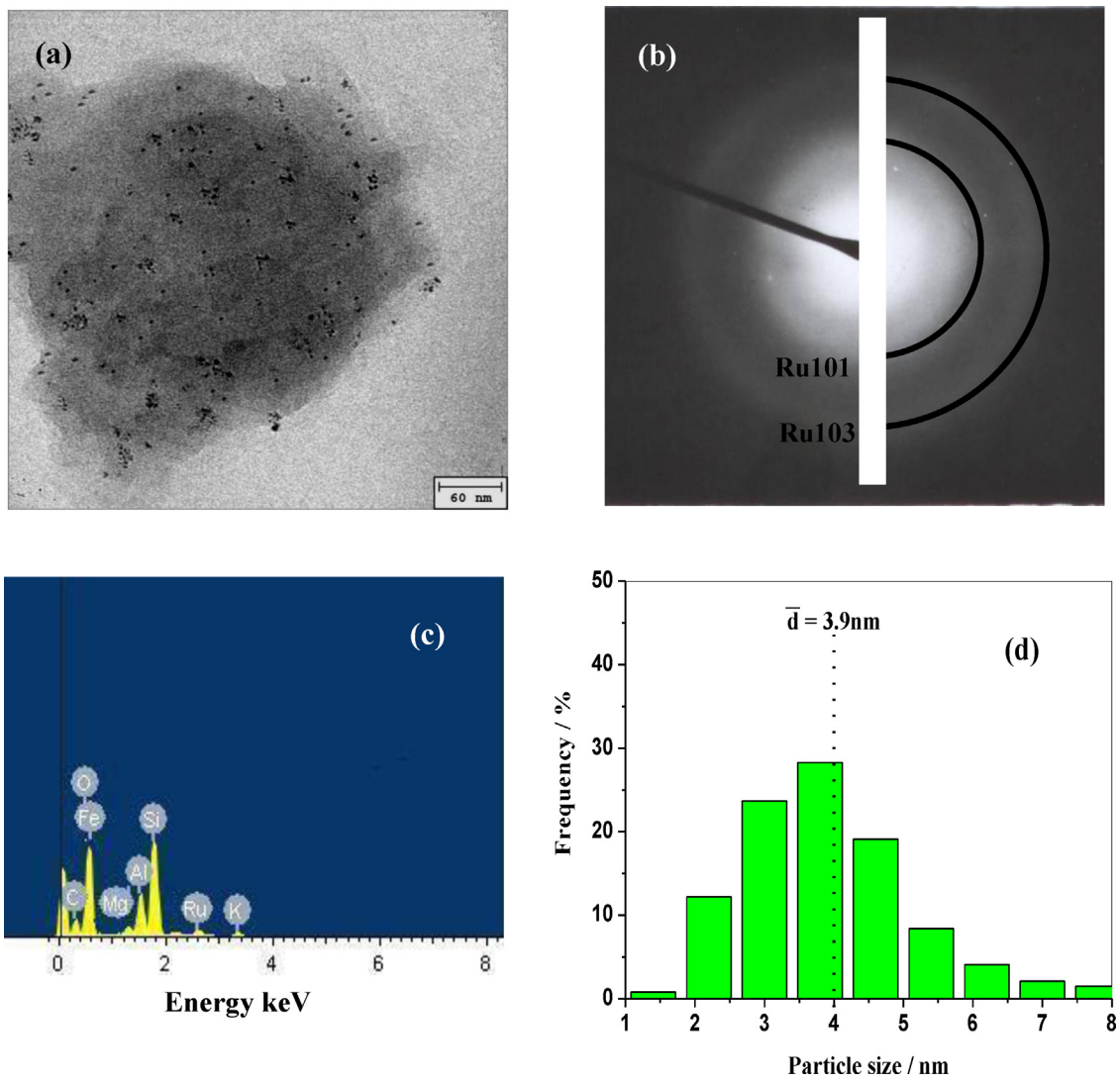

Fig. 3. TEM image (a), SAED pattern (b), EDX result (c), and size distribution (d) of the as-prepared Ru/MMT catalyst.

primarily depends on the catalyst activities. However, factors such as $NaBH_4$ loading, catalyst amount, and temperature also play significant roles in the hydrolysis of $NaBH_4$. These factors were studied and discussed in the subsequent sections.

3.2.1. Catalytic activity of Ru/MMT

Fig. 5 shows a typical plot of the H_2 volumes generated as a function of time from an alkaline $NaBH_4$ solution as catalyzed by 32 mg Ru/MMT and Na-MMT in the presence of 1 wt% $NaBH_4$ and 3 wt% NaOH at 25 °C. With Na-MMT, nearly no H_2 generation occurred. Therefore, the catalytic effect of Na-MMT on H_2 generation was negligible in this study. In the case of Ru/MMT, a linear hydrogen generation started and continued until completion without induction period, and its high linear dependence without any time lag during the initial stages of H_2 generation enables a sustainable and controllable H_2-release process for practical applications. It was found that the hydrogen was completely released within 1000 s in the system with 32 mg Ru/MMT catalyst ($Ru/NaBH_4$ molar ratio = 0.002), with an average rate of hydrogen evolution of $28{,}500 \pm 500\ mL\ min^{-1}\ g(Ru)^{-1}$ at 25 °C. The comparisons of catalytic activities of Ru/MMT with those of other Ru-based heterogeneous catalysts used for the hydrolysis of $NaBH_4$ solution are listed in Table 1. It is found that the H_2 generations rate of Ru/MMT catalyst is much higher than those of most Ru-based catalysts in basic solution [41–47], such as Ru/IRA-120, Ru/Carbon, $Ru/\gamma\text{-}Al_2O_3$, etc. and comparable with $LiCoO_2$ supported Ru [48], IRA-400 supported Ru [49], and graphite supported Ru [50], demonstrating that Ru/MMT is a highly active catalyst for $NaBH_4$ hydrolysis.

3.2.2. Effect of the Ru/MMT amount

The effect of the Ru/MMT amount (8.3, 16, 24.2, and 32.5 mg) in the presence of 1 wt% $NaBH_4$ and 3 wt% NaOH on the H_2 generation rate at 25 °C is plotted in Fig. 6(a). It could be seen that the addition of Ru/MMT catalyst, even at a small amount, immediately initiated the hydrolysis reaction of $NaBH_4$ with no appreciable induction period. The reaction time required for completing the hydrolysis reaction was reduced with increasing catalyst amount. Fig. 6(b) plotted the H_2 generation rate against the Ru concentration, both in logarithmic scales. And the plot yields a best-fit straight line (correlation coefficient, $R^2 = 0.977$) with a slope of $1.13 \approx 1$, indicating that the hydrolysis reaction is first-order with respect to the Ru/MMT amount. A similar finding was also reported by Zahmakiran and Özkar [51] in their study of the hydrolysis of $NaBH_4$ as catalyzed by intrazeolite Ru nanoclusters (Ru/zeolite-Y). But there existed a noticeable induction period in Ru/zeolite-Y, which was due to the inaccessibility of Ru nanoclusters by borohydride ions through cavities. Compared with Ru/zeolite-Y catalyst, the Ru/MMT catalyst minimized the accessibility, and made for higher catalytic activity.

Table 1
Activation energy (E_a) and catalytic activity for various Ru-based heterogeneous catalyst systems used for the hydrolysis of $NaBH_4$ solution.

Catalyst/support	Ru loading (wt%)	Catalyst dosage (mg)	NaOH (wt%)	$NaBH_4$ (wt%)	Tem. (°C)	E_a (kJ mol^{-1})	Activity (mL H_2/min/g $_{Ru}$)[c]	Ref.
Ru/MMT	1.91	32	3	1	25	54.5	28,500	This work
Ru/IRA-120	1	200	1	5	25	49.7	13,200[a]	41
Ru/Carbon	3	200	3.75	0.993	25	66.9	12,900[a]	42
Ru/Carbon	3	3000	0	15	26	37.3	10,870[b]	43
Ru/IRA-400	5	250	10	20	25	47	3772[a]	44
Ru/ZrO_2-SO_4	1	250	4	2	24	76	9,100[b]	45
Ru/γ-Al_2O_3	2.3	500	1	12	30	54.9	1,618[b]	46
Ru/Pst	3.1	100	1	1	Not stated	Not stated	7203[b]	47
Ru/$LiCoO_2$	0.93	20	5	10	25	68.5	32,258[b]	48
Ru/IRA-400	5	250	1	7.5	25	56	30,240[b]	49
Ru/Graphite	3	100	5	10	30	61.1	32,300[a]	50
Ru/zeolite-Y	0.8	316	5	0.56	25	34.9	16,130[a]	51
Ru/zeolite-Y	0.72	351	0	0.56	25	49	133,072[a]	51

[a] As provided by the literature.
[b] As calculated by the author based on the literature.
[c] Activity refers to the initial hydrogen generation rate of $NaBH_4$ hydrolysis.

3.2.3. *Effect of $NaBH_4$ loading*

The effect of $NaBH_4$ loading (1, 3, 5, and 10 wt%) in the presence of 3 wt% NaOH and 8 mg Ru/MMT catalyst on the H_2 generation rate at 25 °C is shown in Fig. 7(a). It could be seen that a linear dependence between the amount of hydrogen generation and reaction time in the course of the reaction was observed, indicating that such a $NaBH_4$ hydrolysis reaction was of the zero-order in substrate concentration and there was no deviation from the zeroth order. This phenomenon is consistent with those of previous studies [52,53]. Actually, the rate of H_2 generation seemed independent of the $NaBH_4$ loading according to our observations. Fig. 7(a) shows that the $NaBH_4$ loading increased from 1 wt% to 10 wt% (a ninefold increase). However, the H_2 generation rate only increased by 26.7%.

To quantitatively evaluate the effect of $NaBH_4$ loading on the rate of H_2 generation, the H_2 generation rate was plotted against $NaBH_4$ loading, with both in logarithmic scales [Fig. 7(b)]. The plot yields a well-fitted straight line (correlation coefficient, $R^2 = 0.918$) with a slope of $0.08 \approx 0$. This result further conforms that the hydrolysis reaction is zero-order with respect to the $NaBH_4$ loading. Thus, the rate law for the hydrolysis of an alkaline $NaBH_4$ solution catalyzed by a Ru/MMT catalyst can be expressed as follows [Eq. (1)]:

$$\frac{-4d[NaBH_4]}{dt} = \frac{d[H_2]}{dt} = k[Ru] \quad (1)$$

where k is the rate constant. In general, the $NaBH_4$ loading would affect the reaction kinetics of $NaBH_4$ hydrolysis, which can be attributed to the increase in the solution viscosity as a result of water consumption as well as the increase in the metaborate by-product concentration [54]. In this study, the zero-order kinetics of $NaBH_4$ loading should be limited to below 10 wt%.

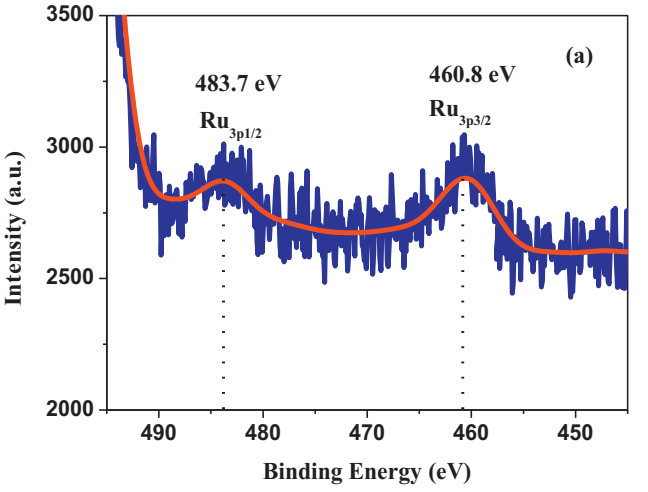

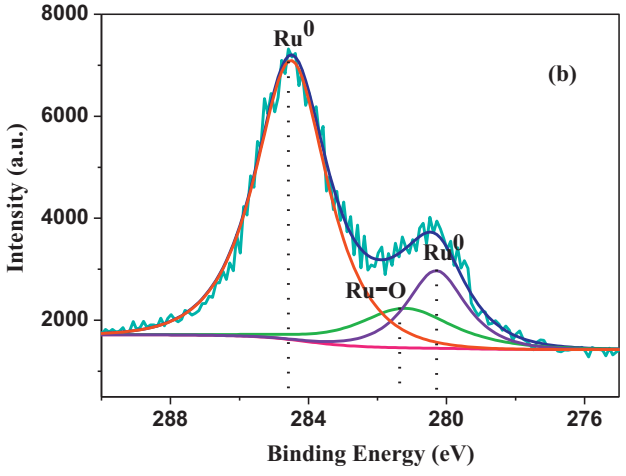

Fig. 4. High-resolution XPS spectra at the Ru 3p edge (a) and Ru 3d edge (b) of the as-prepared Ru/MMT catalyst.

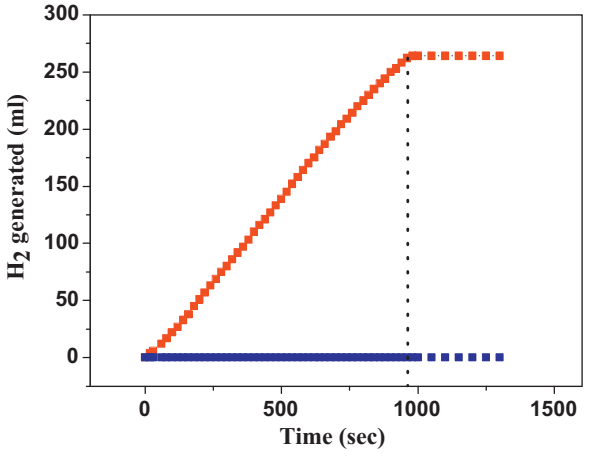

Fig. 5. Volume of H_2 generated as a function of time measured from 1 wt% $NaBH_4$ + 3 wt% NaOH solution at 25 °C using 32 mg of Ru/MMT and 32 mg of Na-MMT.

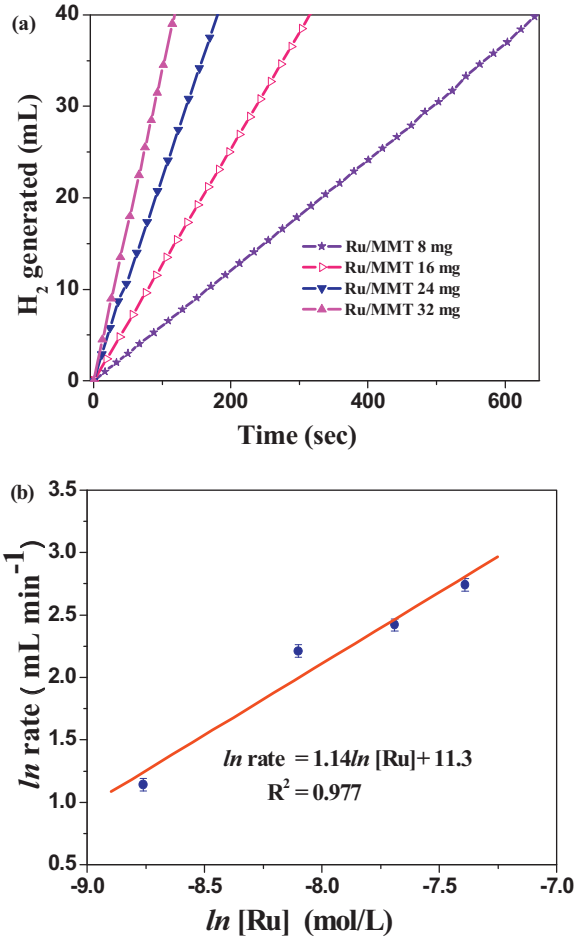

Fig. 6. (a) Volume of H_2 generated as a function of the Ru/MMT catalyst amount measured from 1 wt% $NaBH_4$ and 3 wt% NaOH at 25 °C. (b) The plot of H_2 generation rate versus the Ru/MMT catalyst concentration (both in logarithmic scale) for the hydrolysis of $NaBH_4$. The error bars on the plot reflect an around ±5% measurement error of the H_2 generation rate.

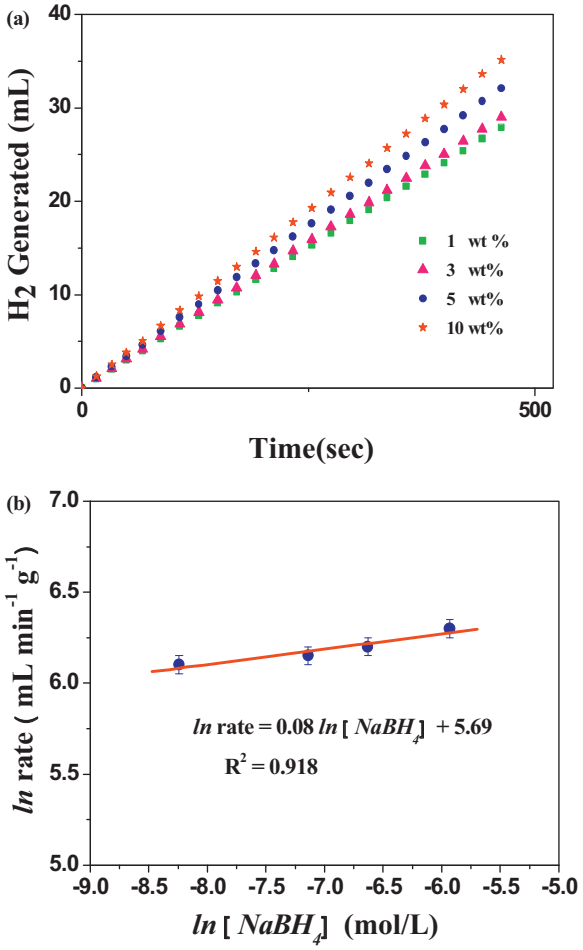

Fig. 7. (a) Volume of H_2 generated as a function of the $NaBH_4$ amount measured from 3 wt% NaOH + 8 mg of Ru/MMT catalyst at 25 °C with various amount of $NaBH_4$. (b) The plot of H_2 generation specific rate versus the $NaBH_4$ concentration (both in logarithmic scale) for the hydrolysis of $NaBH_4$. The error bars on the plot reflect an around ±5% measurement error of the H_2 generation rate.

3.2.4. Effect of temperature

Temperature is known to play an important role in hydrogen generation process. The effect of temperature on catalytic activity was further investigated at different temperatures. Fig. 8(a) shows the effects of different temperatures (from 10 °C to 30 °C) on the H_2 generation rate in solutions containing 1 wt% $NaBH_4$ + 3 wt% NaOH and 32 mg of Ru/MMT catalyst. As expected, an increase in the temperature results in higher H_2 generation rates. When the temperature increased from 10 °C to 30 °C, an apparent increase in the H_2 generation rate from 7173 mL min^{-1} g(Ru)$^{-1}$ to 34660 mL min^{-1} g(Ru)$^{-1}$ was observed. Fig. 8(b) shows the Arrhenius plot, ln k versus the reciprocal absolute temperate ($1/T$). The apparent E_a for the Ru/MMT-catalyzed hydrolysis of $NaBH_4$ was estimated as 54.5 ± 1 kJ/mol.

Table 1 lists the E_a for the hydrolysis reaction of the $NaBH_4$ solution as catalyzed by other Ru-based catalysts for comparison. Apart from the 47 kJ/mol for Ru/IRA-400 [44], 49.7 kJ/mol for Ru/IRA-120 [41], 37.3 kJ/mol for Ru/carbon [43], and 34.9 kJ/mol for Ru/zeolite [51], the Ru/MMT catalyst provides the lowest E_a value for the hydrolysis for $NaBH_4$. Shang et al. thought the kinetics changes with the catalyst, $NaBH_4$, and NaOH concentrations as well as with the solution temperature and reaction time span [55]. Given the different test conditions for the kinetic study of $NaBH_4$ hydrolysis over various catalysts in Table 1, the conduct of an exact comparison is not enough merely based on the E_a value. If the catalytic activity data was also considered, the Ru/MMT catalyst showed the highest catalytic activity among the catalysts with the lower E_a values than Ru/MMT. The Ru/MMT catalyst showed high catalytic activity in $NaBH_4$ hydrolysis because of two reasons: one is the high dispersion of the Ru nanoparticles in the clay mineral matrix, and the other is the open framework structure of MMT, which can significantly reduce the substrate inhibition.

3.3. Ru/MMT catalyst reusability

Catalyst reusability is crucial in the practical application of the H_2 generation process. In the present study, the reusability of the Ru/MMT catalyst was determined by repeating the same catalyzed hydrolysis experiment ten times using the same catalyst batch. After each run, the catalyst was collected and thoroughly washed with deionized water using centrifugation. Fig. 9 shows the H_2 generation rate as a function of the cycle times in a solution containing 1 wt% $NaBH_4$ + 3 wt% NaOH and 32 mg Ru/MMT catalyst at 25 °C. The H_2 generation rate gradually decreased from ca. 637 mL min^{-1} g^{-1} initially to ca. 312 mL min^{-1} g^{-1} during the H_2 production process; only 49% of the initial H_2 generation rate was observed after 10 runs. The reduced activity of the catalysts in the hydrolysis of $NaBH_4$ during cycle test was also observed by Zahmakiran and Özkar [51] in their study of Ru/zeolite-Y, Liang et al. [50] in their study of Ru/Graphite, Chen et al. [47] in their study of Ru/polymer, and Pinto et al. [56] in their study of Ni–Ru powder.

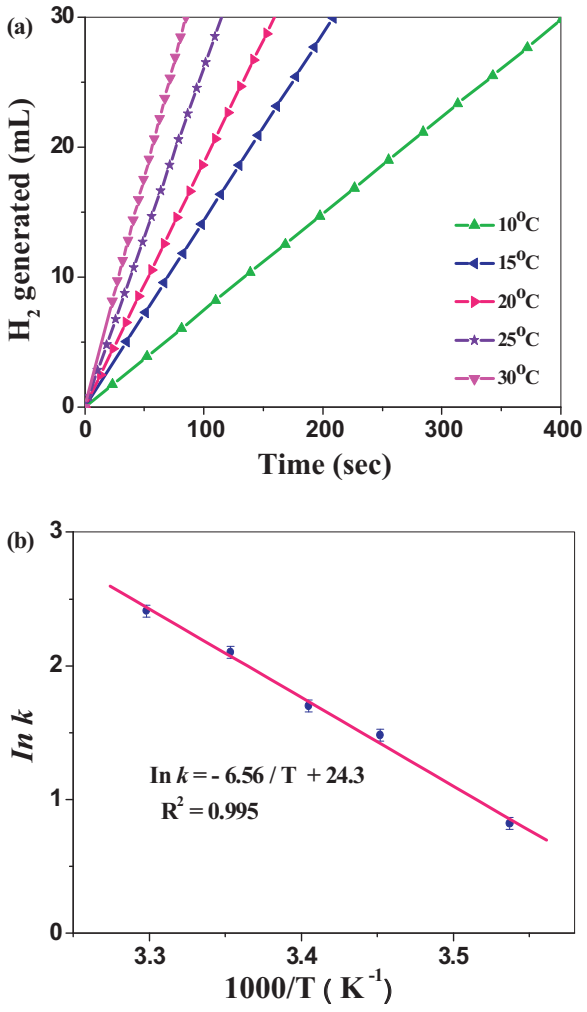

Fig. 8. (a) Volume of H_2 generated as a function of temperature measured from 1 wt% $NaBH_4$ + 3 wt% NaOH solution + 32 mg of Ru/MMT catalyst. (b) ln k vs. $1/T$ plot for the H_2 generation reaction. The error bars on the plot reflect an around ±5% measurement error of the H_2 generation rate.

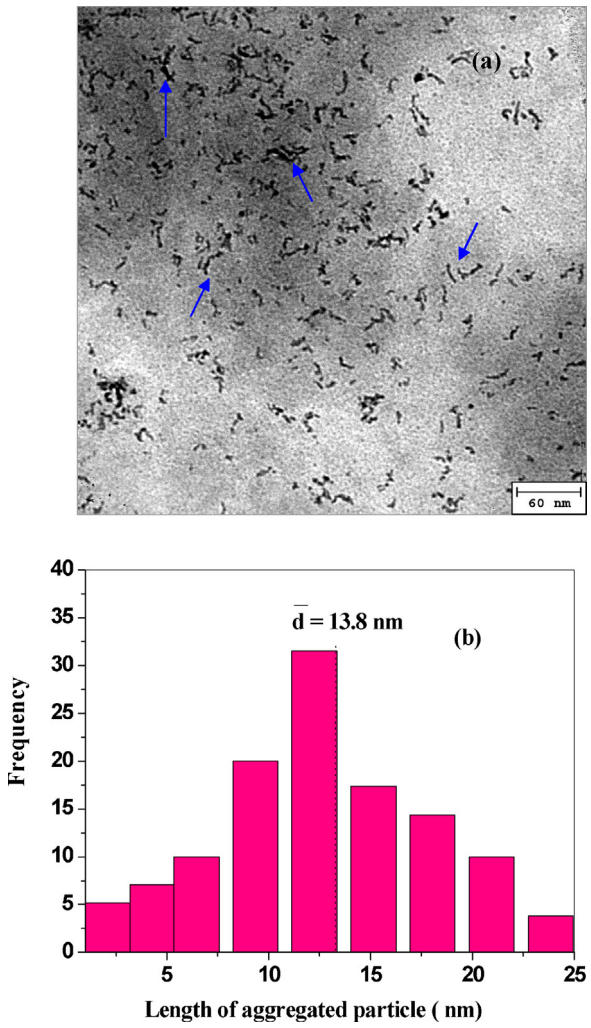

Fig. 10. TEM image (a) and size distribution (b) of the Ru/MMT catalyst after ten runs.

However, studies on the physical and chemical processes that contribute to this activity loss are limited [57]. Therefore, the catalyst degradation mechanism in $NaBH_4$ hydrolysis in an alkaline solution remains unclear. Attempts have been made to elucidate the activity loss of the Ru/MMT catalyst using TEM, FESEM, BET, and XPS analyses.

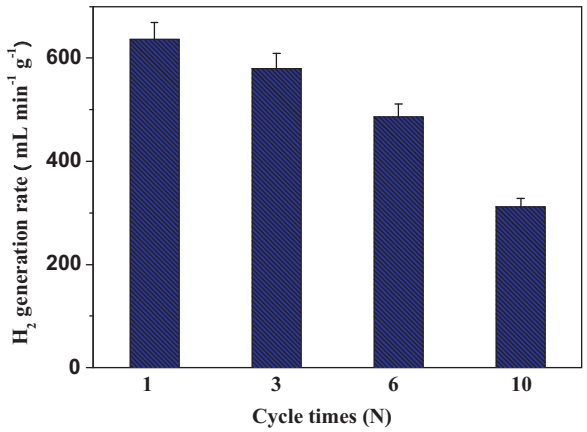

Fig. 9. Cyclic performance of the Ru/MMT catalyst in catalyzing the hydrolysis of alkaline $NaBH_4$ solution measured from 1 wt% $NaBH_4$ and 3 wt% NaOH at 25 °C.

3.3.1. *Ru nanoparticle aggregation*

Fig. 10 shows the TEM image and the size distribution of the deposited Ru nanoparticles in the MMT matrix after 10 runs. The arrows in Fig. 10(a) indicate a worm-like morphology that is due to the aggregation of the Ru nanoparticles deposited on the external surface of MMT. The length of aggregated particle (Fig. 10b) of the deposited Ru nanoparticles ranged from 2.1 nm to 25.9 nm, with an average value of 13.8 nm. Compared with the 3.9 nm size of the as-prepared Ru/MMT (Table 2), the size of the Ru nanoparticles in the reused Ru/MMT catalyst clearly was increased after 10 cycles. Accordingly, one of the reasons responsible for the degradation of the catalytic activity can be attributed to the aggregation of the Ru nanoparticles deposited on the external surface of MMT. Similar conclusions were also reported by Miao et al. in their study of the Ru/MMT-catalyzed hydrogenation of benzene [58], by Dai et al. in their study of the Ru/MMT-catalyzed hydrolysis of ammonia borane [35], and by Kim et al. in their study of the use of a filamentary Ni catalyst in $NaBH_4$ hydrolysis [59].

3.3.2. *Ru nanoparticle fall-off*

The morphology and composition of the catalysts before and after 10 catalytic cycles were determined using FESEM (Fig. 11)

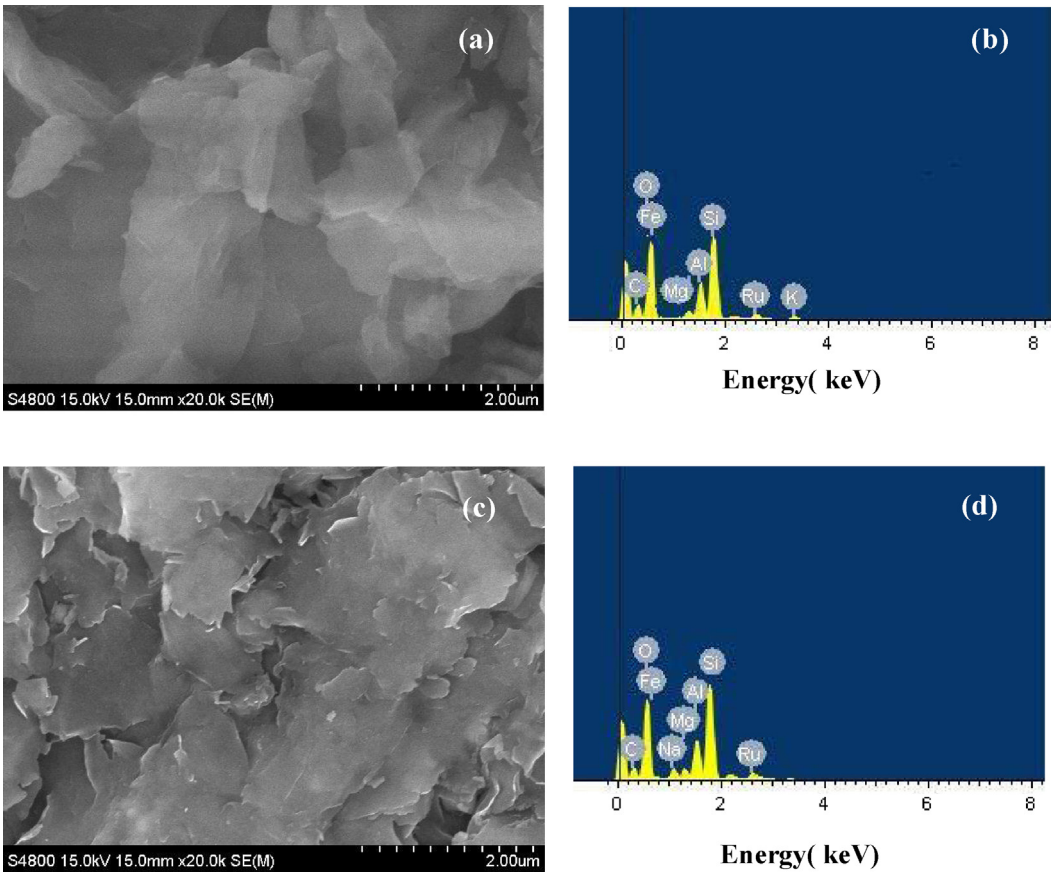

Fig. 11. FESEM images and EDX results of the as-prepared Ru/MMT catalyst (a and b) and Ru/MMT catalyst after ten runs (c and d), respectively.

to elucidate the degradation mechanism of the Ru/MMT catalyst further. As indicated by Fig. 11(a) and (c), the morphology of the Ru/MMT catalyst before and after 10 runs showed clear differences: the layer sheets of the as-prepared Ru/MMT consisted of a higher number of stacking layer compared with those of the catalyst after 10 runs. The layer sheets were exfoliated and became thinner during the catalytic cycles as a result of the strong alkaline surrounding [60]. After 10 runs, the Ru/MMT catalyst exhibited higher dispersion in water than the as-prepared Ru/MMT because of the thinner layer sheets of the former. Thus, this phenomenon provides experimental evidence for the existence of these thin layer sheets. Aside from the morphological changes, the composition of the two catalysts also changed, as shown by the corresponding EDX results (Fig. 11b and d). Two distinct differences were observed: one is the appearance of Na and the disappearance of K in the Ru/MMT catalyst after 10 runs; the other is the decrease in the Ru content of the reused catalyst (Table 2). As further determined by ICP, the Ru content from 1.91 wt% of the as-prepared catalyst to 1.83 wt% of the Ru/MMT catalyst after 10 runs, indicating that approximately 4.2 wt% of Ru was unaccounted for during the catalytic cycles. The partial fall-off of the Ru nanoparticles from the MMT matrix might be the high concentrations of NaOH and $NaBH_4$ during the catalytic cycles, which drive the fall-off of Ru nanoparticles from the MMT matrix. The FESEM, EDX and ICP results show that the second factor mainly responsible for the degradation of the catalytic activity is the partial fall-off of the Ru nanoparticles. A similar conclusion was reported by Chen and co-workers in their study of the Ru-immobilized polymer-supported catalyst (Ru/Pst) for $NaBH_4$ hydrolysis [55].

3.3.3. Decrease in the catalyst specific area

As previously mentioned, aggregation of the Ru nanoparticles deposited on the external surface of MMT were observed during catalytic cycles. The phenomenon was expected to result in a decrease in the specific surface area of the catalyst. For clarification, the specific surface areas of the as-prepared catalyst and that after 10 runs were measured and compared. Fig. 12 shows that both catalysts exhibited type-IV adsorption–desorption characteristics. Generally speaking, the specific surface area of MMT obtained by BET is merely external surface. According to the N_2 adsorption data, the specific surface areas of the Ru/MMT catalysts before and after 10 runs were 47.6 and 43.2 $m^2\,g^{-1}$, as listed in Table 2. The specific surface area decreased by 9.2% after 10 cycles, showing a slight decrease in the specific surface. In their study of the Ru/MMT-catalyzed hydrolysis of ammonia borane [35], Dai et al. proposed that the slight decrease (11.8%) in the specific surface area is due to the incorporation of the residual by-product ($NaBO_2$) in the MMT mesopores. In their study of the $PtRu/LiCoO_2$-catalyzed

Table 2
The comparison between the as-prepared Ru/MMT catalyst and the Ru/MMT catalyst after ten runs.

Samples	Ru (%)[a]	Ru (%)[b]	Particle size (nm)	BET (m^2/g)
As-prepared catalyst	1.91	2.21	3.9	47.6
Reused catalyst	1.83	1.78	13.8	43.2

[a] As determined by ICP.
[b] As determined by EDX.

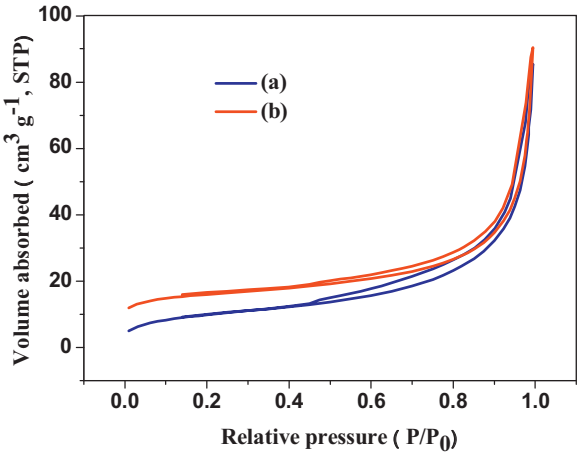

Fig. 12. Nitrogen adsorption–desorption isotherms of the as-prepared Ru/MMT catalyst (a) and Ru/MMT catalyst after ten runs (b), respectively.

hydrolysis of $NaBH_4$ [61], Krishnan et al. found that cobalt boride can be formed during the catalytic reaction. To determine whether the B composition existed in the Ru/MMT catalyst after 10 runs, XPS analysis, which is a powerful technique for determining surface states, was performed to investigate the chemical changes on the surface of the Ru/MMT catalyst after 10 runs. Fig. 13 shows the survey XPS spectrum of the Ru/MMT catalyst after 10 runs. According to literature, the peak of the B composition is assigned to 193 eV [61]; this peak is obviously absent in the inset of Fig. 13. Therefore, the slight decrease in the specific surface area of the Ru/MMT catalyst after 10 runs was not caused by the incorporation of the residual by-product ($NaBO_2$) in the MMT mesopores. The formation of ruthenium boride (RuB) during the catalytic cycles was also excluded. Instead, the slight decrease in the specific surface areas should attribute to the aggregation of Ru nanoparticles during catalytic cycles, indicating a reduction in the number of reactive sites. But the slight decrease in the specific surface areas also indicated that the extent of aggregation was not so serious, which further confirmed the good stability of Ru/MMT during catalytic cycles due to the well dispersing action of MMT. Accordingly, the third factor responsible for the degradation of the catalytic activity is the reduction in the number of reactive sites. This reduction is due to the agglomeration of the Ru nanoparticles deposited on the external surface of MMT.

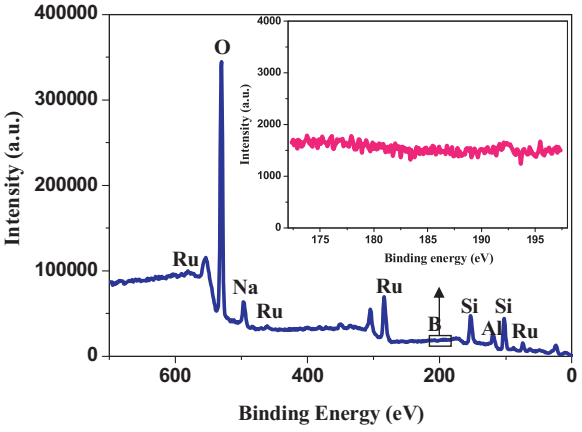

Fig. 13. Survey XPS spectrum of the reused Ru/MMT catalyst. The inset shows the XPS spectrum of B.

4. Conclusions

The Ru nanoparticles deposited on the external surface of MMT (Ru/MMT) were successfully prepared by an in situ wet chemical reduction. The deposited Ru nanoparticles were well dispersed and showed good stability during catalytic cycles due to the well dispersing action of MMT. The use of the as-prepared catalyst in a 1 wt% $NaBH_4$ + 3 wt% NaOH solution produced an average H_2 generation rate of 28,500 ± 500 mL min^{-1} $g(Ru)^{-1}$ at 25 °C. The apparent E_a of the $NaBH_4$ hydrolysis reaction was 54.5 ± 1 kJ/mol, which was lower than most of Ru-based heterogeneous catalysts reported in literatures. The catalytic activity of the Ru/MMT catalyst gradually decreased with cycling; only 49% of the initial H_2 generation rate remained after 10 runs. TEM, FESEM, ICP, BET, and XPS analyses were performed before and after 10 reutilizations to determine the deterioration mechanism of the Ru/MMT catalyst during the catalytic cycles. TEM, FESEM, and ICP results show the aggregation and partial fall-off of the Ru nanoparticles deposited on the external surface of MMT in the reused catalyst. In addition, the BET data reveal a 9.2% decrease in the specific surface area of the catalyst after 10 cycles. The slight decrease in the specific surface area of the reused Ru/MMT catalyst was not caused by the incorporation of the residual by-product ($NaBO_2$) or by the formation of RuB, as confirmed by XPS analysis. Instead, the deterioration of the reused catalyst may have been caused by the aggregation of the Ru nanoparticles. A more robust catalyst is necessary to prevent the aggregation and partial fall-off of the Ru nanoparticles. Future studies should include the introduction of an organic molecule with a chelating group (which can act as the coordinating sites for Ru^{3+} ion chelation) on the surface of the support to construct organic–inorganic hybrid materials. The introduction of this group is expected to result in the strong attachment and high durability of Ru or other metal nanoclusters during the catalytic cycles.

Acknowledgements

This work was financially supported by National Natural Science Foundation of China (No: 21101058, 41171369, and 21076063).

References

[1] B.H. Liu, Z.P. Li, Journal of Power Sources 187 (2009) 527–534.
[2] D.M.F. Santos, C.A.C. Sequeira, Renewable and Sustainable Energy Reviews 15 (2011) 3980–4001.
[3] L. Schlapbach, A. Züttel, Nature 414 (2001) 353–358.
[4] J.-H. Wee, K.-Y. Lee, S.H. Kim, Fuel Processing Technology 87 (2006) 811–819.
[5] Y. Kojima, K. Suzuki, K. Fukumoto, Y. Kawai, M. Kimbara, H. Nakanishi, S. Matsumoto, Journal of Power Sources 125 (2004) 22–26.
[6] H.K. Atiyeh, B.R. Davis, International Journal of Hydrogen Energy 32 (2007) 229–236.
[7] H.I. Schlesinher, H.C. Brown, A.E. Finhoil, J.R. Gilbreath, H.R. Hoekstra, E.K. Hyde, Journal of the American Chemical Society 75 (1953) 215–262.
[8] Y. Kojima, K. Suzuki, K. Fukumoto, M. Sasaki, T. Yamamoto, Y. Kawai, H. Hayashi, International Journal of Hydrogen Energy 27 (2002) 1029–1034.
[9] V.I. Simagina, P.A. Storozhenko, O.V. Netskina, O.V. Komova, G.V. Oegova, T.Y. Samoilenko, Kinetics and Catalysis 48 (2007) 168–175.
[10] S. Peng, J. Liu, X. Liu, Y. Zhang, J. Zhang, Advanced Materials Research 197–198 (2011) 1577–1581.
[11] O. Metin, S. Özkar, Journal of Molecular Catalysis A: Chemical 295 (2008) 39–46.
[12] M. Rakap, S. Özkar, Applied Catalysis B: Environmental 91 (2009) 21–29.
[13] N. Sahiner, O. Ozay, E. Inger, N. Aktas, Applied Catalysis B: Environmental 102 (2011) 201–206.
[14] C.-H. Liu, B.-H. Chen, C.-L. Hsueh, J.-R. Ku, F. Tsau, K.-J. Hwang, Applied Catalysis B: Environmental 91 (2009) 368–379.
[15] K.S. Eom, K.W. Cho, H.S. Kwon, Journal of Power Sources 180 (2008) 484–490.
[16] P. Krishnan, S.G. Advani, A.K. Prasad, Applied Catalysis B: Environmental 86 (2009) 137–144.
[17] J.C. Ingersoll, N. Main, J.C. Thenmozhiyal, A. Muthaiah, Journal of Power Sources 173 (2007) 450–457.
[18] H.B. Dai, Y. Li, P. Wang, X.D. Yao, T. Rufford, M. Lu, H.M. Cheng, International Journal of Hydrogen Energy 33 (2008) 4405–4412.
[19] N. Patel, R. Fernanes, A. Miotello, Journal of Catalysis 27 (2010) 315–324.

[20] R. Peña-Alonso, A. Sicurelli, E. Callone, G. Carturan, R. Raj, Journal of Power Sources 165 (2007) 315–323.
[21] G.M. Arzac, T.C. Rojas, A. Fernández, Applied Catalysis B: Environmental 128 (2012) 39–47.
[22] R. Fernandes, N. Patel, A. Miotello, International Journal of Hydrogen Energy 34 (2009) 2893–2900.
[23] H.C. Brown, C.A. Brown, Journal of the American Chemical Society 84 (1962) 1493–1494.
[24] U.B. Demirci, F. Garin, Journal of Alloys and Compounds 463 (2008) 107–111.
[25] M. Zahmakiran, S. Özkar, Langmuir 24 (2008) 7065–7067.
[26] M. Zahmakiran, S. Özkar, Journal of Molecular Catalysis A: Chemical 258 (2006) 95–103.
[27] S. Özkar, M. Zahmakiran, Journal of Alloys and Compounds, 404-406 (2005) 728–731.
[28] C. Crisafulli, S. Scirè, M. Salanitri, R. Zito, S. Calamia, International Journal of Hydrogen Energy 36 (2011) 3817–3826.
[29] L. Saikia, D. Dutta, D.K. Dutta, Catalysis Communications 19 (2012) 1–4.
[30] L.A. Galeano, A. Gil, M.IA. Vicente, Applied Catalysis B: Environmental 104 (2011) 252–260.
[31] J. Ma, J. Zou, L. Li, C. Yao, T. Zhang, D. Li, Applied Catalysis B: Environmental 134–135 (2013) 1–6.
[32] B.S. Kadu, Y.D. Sathe, A.B. Ingle, R.C. Chikate, K.R. Patil, C.V. Rode, Applied Catalysis B: Environmental 104 (2011) 407–414.
[33] H. Tian, Q. Guo, D. Xu, Journal of Power Sources 195 (2010) 2136–2142.
[34] R. Chamoun, B. Demirci, D. Cornu, Y. Zaatar, R. Khoury, A. Khoury, P. Miele, Fuel 90 (2011) 1919–1926.
[35] H.-B. Dai, X.-D. Kang, P. Wang, International Journal of Hydrogen Energy 35 (2010) 10317–10323.
[36] S.C. Amendola, M. Binder, S.L. Sharp-Goldman, M.T. Kelly, P.J. Petillo, U.S. Pat. 6,683,025 B2; Jan 27, 2004.
[37] M. Fan, P. Yuan, F. Bergaya, H. He, T. Chen, J. Zhu, D. Liu, Clays and Clay Minerals 59 (2011) 490–500.
[38] P. Sivakumar, R. Ishak, V. Tricoli, Electrochimica Acta 50 (2005) 3312–3319.
[39] S. Peng, C. Liu, X. Liu, J. Zhang, Y. Zhang, Integrated Ferroelectrics 135 (2012) 47–54.
[40] M.M. Kreevoy, R.W. Jacobson, Ventron Alembic 15 (1979) 2–3.
[41] C.L. Hsueh, C.Y. Chen, J.R. Ku, S.F. Tsai, Y.Y. Hsu, F.H. Tsau, M.S. Jeng, Journal of Power Sources 177 (2008) 485–492.
[42] J.S. Zhang, W.N. Delgass, T.S. Fisher, J.P. Gore, Journal of Power Sources 164 (2007) 772–781.
[43] Y.H. Shang, R. Chen, Energy and Fuels 20 (2006) 2149–2154.
[44] S.C. Amendola, S.L. Sharp-Goldman, M.S. Janjua, M.T. Kelly, P.J. Petillo, M. Binder, Journal of Power Sources 85 (2000) 186–189.
[45] U.B. Demirci, F. Garin, Journal of Molecular Catalysis A: Chemical 279 (2008) 57–62.
[46] A.J. Huang, S.F. Tsai, Y.Y. Hsu, J.R. Ku, Y.H. Chen, C.C. Yu, International Journal of Hydrogen Energy 33 (2008) 6205–6215.
[47] C.W. Chen, C.Y. Chen, Y.H. Huang, International Journal of Hydrogen Energy 34 (2009) 2164–2173.
[48] Z. Liu, B. Guo, S.H. Chan, E.H. Tang, L. Hong, Journal of Power Sources 176 (2008) 306–311.
[49] S.C. Amendola, S.L. Sharp-Goldman, M.S. Janjua, N.C. Spencer, M.T. Kelly, P.J. Petillo, M. Binder, International Journal of Hydrogen Energy 25 (2000) 969–975.
[50] Y. Liang, H.-B. Dai, L.-P. Ma, P. Wang, H.-M. Cheng, International Journal of Hydrogen Energy 35 (2010) 3023–3028.
[51] M. Zahmakiran, S. Özkar, Langmuir 25 (2009) 2667–2678.
[52] D. Xu, P. Dai, Q. Guo, X. Yue, International Journal of Hydrogen Energy 33 (2008) 7371–7377.
[53] W. Ye, H. Zhang, D. Xu, L. Ma, B. Yi, Journal of Power Sources 164 (2007) 644–648.
[54] R. Retnamma, A.Q. Novais, C.M. Rangel, International Journal of Hydrogen Energy 36 (2011) 9772–9790.
[55] Y. Shang, R. Chen, C. Jiang, International Journal of Hydrogen Energy 33 (2008) 6719–6726.
[56] A.M.F.R. Pinto, M.J.F. Ferreira, V.R. Fernandes, C.M. Rangel, Catalysis Today 170 (2011) 40–49.
[57] S.S. Muir, X. Yao, International Journal of Hydrogen Energy 36 (2011) 5983–5997.
[58] S. Miao, Z. Liu, B. Han, J. Huang, Z. Sun, J. Zhang, T. Jiang, Angewandte Chemie International Edition 45 (2006) 266–269.
[59] J.-H. Kim, K.-T. Kim, Y.-M. Kang, H.-S. Kim, M.-S. Song, Y.-J. Lee, P.S. Lee, J.-Y. Lee, Jounal of Alloys and Compounds 379 (2004) 222–227.
[60] S. Peng, Q. Gao, Z. Du, J. Shi, Applied Clay Science 31 (2006) 229–237.
[61] P. Krishnan, K.-L. Hsueh, S.-D. Yim, Applied Catalysis B: Environmental 77 (2007) 206–214.